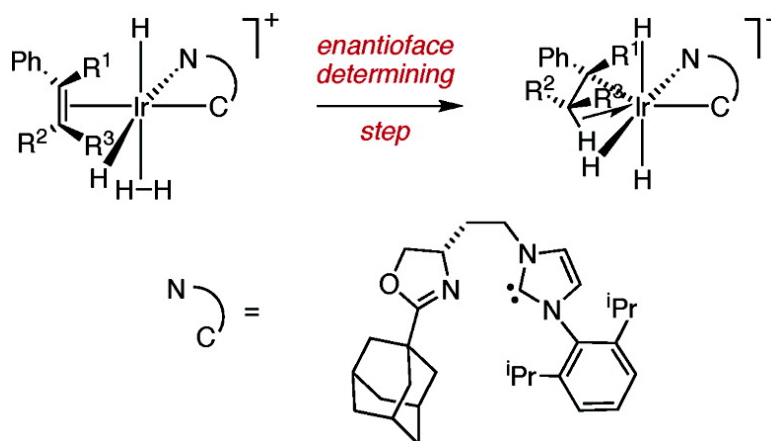


## Electronic Effects Steer the Mechanism of Asymmetric Hydrogenations of Unfunctionalized Aryl-Substituted Alkenes

Yubo Fan, Xiuhua Cui, Kevin Burgess, and Michael B. Hall

*J. Am. Chem. Soc.*, **2004**, 126 (51), 16688-16689 • DOI: 10.1021/ja044240g • Publication Date (Web): 04 December 2004

Downloaded from <http://pubs.acs.org> on April 5, 2009



### More About This Article

Additional resources and features associated with this article are available within the HTML version:

- Supporting Information
- Links to the 3 articles that cite this article, as of the time of this article download
- Access to high resolution figures
- Links to articles and content related to this article
- Copyright permission to reproduce figures and/or text from this article

[View the Full Text HTML](#)

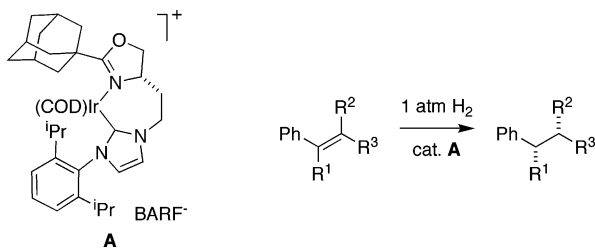
## Electronic Effects Steer the Mechanism of Asymmetric Hydrogenations of Unfunctionalized Aryl-Substituted Alkenes

Yubo Fan, Xiuhua Cui, Kevin Burgess,\* and Michael B. Hall\*

Department of Chemistry, Texas A & M University, Box 30012, College Station, Texas 77842-3012

Received September 22, 2004; E-mail: burgess@tamu.edu

Cationic iridium(I) complexes, such as Crabtree's catalyst  $[\text{Ir}(\text{PCy}_3)_3(\text{C}_5\text{NH}_5)(\text{COD})](\text{PF}_6)$ , are fundamentally different from similar rhodium systems insofar as only the former mediate hydrogenation of hindered, largely unfunctionalized alkenes.<sup>1</sup> The scope of such iridium-mediated hydrogenations has been expanded by Pfaltz<sup>2-4</sup> and others<sup>5-7</sup> who demonstrated high conversions and enantioselectivities for several aryl-substituted alkenes. Rational development of the catalysts has, however, been limited by mechanistic uncertainties that surround the reaction; key steps in the catalytic pathway have yet to be identified. Communicated here is an in-depth study of iridium-mediated hydrogenation reactions of trisubstituted arylalkenes via density functional theory (DFT)<sup>8</sup> that reveals those steps for the catalyst **A**, developed in our laboratories.<sup>9,10</sup> We believe these studies do provide a suitable mechanistic model for rational developments in the field.

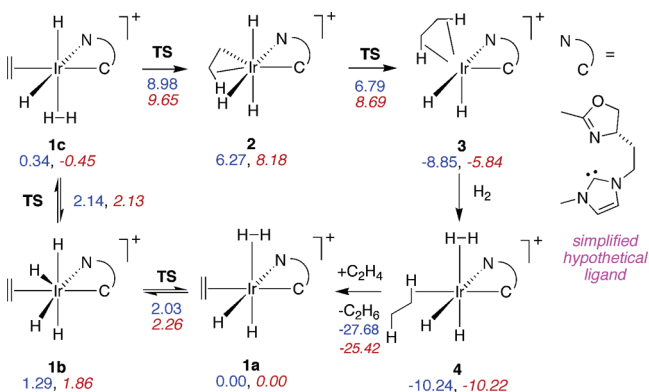


Two levels of theory were used in these studies. The first was PBE with LANL2DZ plus density-fitting basis sets, which expand the density in a set of atom-centered functions when computing the Coulomb interaction, instead of computing all of the two-electron integrals, and hugely accelerate pure DFT calculations without a significant degradation in the accuracy. The second was B3LYP with LANL2DZ plus one polarization and one diffuse function. B3LYP was only used to validate the geometries and energies obtained from PBE in selected test cases. Density-fitting basis sets cannot be used with B3LYP; hence, this method is several times slower.

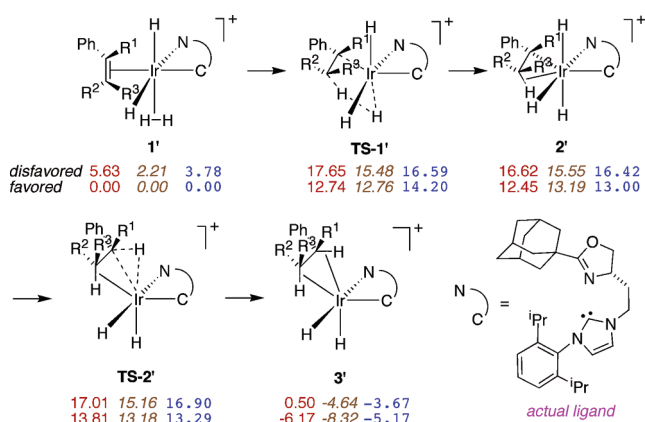
Initially, a model complex was considered wherein methyl groups were substituted for the 2,6-*i*-Pr<sub>2</sub>C<sub>6</sub>H<sub>3</sub> and 1-adamantyl substituents. A comprehensive set of PBE calculations encompassing most of the obvious pathways to product for this complex led to a predicted mechanistic pathway. This featured an Ir(III)/Ir(V) cycle in which a coordinated alkene in intermediate **1** metathetically reacts with a dihydrogen ligand (in preference to a hydride) to form an alkyl complex **2** with a  $\beta$ -agostic interaction. Relatively fast reductive elimination allows the reduced alkene to dissociate via the transient intermediates **3** and **4**. Finally, another alkene molecule enters the catalytic cycle, re-establishing the equilibrium between **1a-c** (Scheme 1).

The relative energies of the intermediates and transition states indicated in Scheme 1 were also calculated at the B3LYP level to test the validity of the PBE approach relative to this higher standard. In fact, the energetics match well. The predicted overall barrier is

**Scheme 1.** Relative Free Energies (kcal mol<sup>-1</sup>) for the Preferred Reaction Pathway Elucidated via PBE (blue) and for the Same Intermediates and Transition States (TS) Calculated via B3LYP (red, italic)



**Scheme 2.** Reaction Pathway Used To Predict Enantioselectivities and Absolute Configurations via PBE Calculations<sup>a</sup>

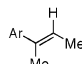
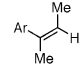
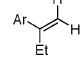


<sup>a</sup>  $\Delta G$  values in kcal mol<sup>-1</sup> listed for (*E*)-2-phenylbut-2-ene (red), (*Z*)-2-phenylbut-2-ene (brown, italic), and 2-phenylbut-1-ene (blue, courier). For the (*Z*)-alkene, the Ph and R<sup>1</sup> substituents are inverted.

slightly higher for B3LYP (9.7 versus 9.0 kcal mol<sup>-1</sup>), and intermediates **2** and **3** are less stable (by 1.9 and 3.0 kcal mol<sup>-1</sup>, respectively), but close nevertheless. Two important conclusions were drawn from these simulations: (i) the PBE method gives satisfactory results, and (ii) both methods predict that the conversion of **1** to **2** is the rate-determining step in the process.

The PBE method was then used to explore the reactions involving the complete ligand of catalyst **A**. Scheme 2 shows the calculated pathways to both enantiomeric products for catalyst **A** and relevant substituents on the alkene. Table 1 shows the alkenes considered, the calculated  $\Delta\Delta G^\ddagger$  values, the predicted configuration of the enantiomers formed, and the corresponding data previously measured experimentally. The experimental data for some substrates

**Table 1.**  $G^\ddagger$  Values and Configurations for Enantioselective Hydrogenations of the Alkenes Indicated

entry	alkene	calculated <sup>a</sup>			experimental <sup>b</sup>	
		$\Delta\Delta G^\ddagger$ <sup>c</sup>	$\Delta\Delta G_{\text{int}}^\ddagger$ <sup>d</sup>	config'n	$\Delta\Delta G^\ddagger$	config'n
1		3.84	4.17	S	2.31	S
2		2.36	2.36	R	1.30	R
3		2.70	3.42	R	1.68	R

<sup>a</sup> Ar = Ph. <sup>b</sup> Ar = 4-MeOC<sub>6</sub>H<sub>4</sub>. <sup>c</sup> Free energy difference of the two highest-energy transition states for the same substrate's two enantiofaces. <sup>d</sup> Free energy difference between the intermediates **2'** for the same substrate's two enantiofaces.

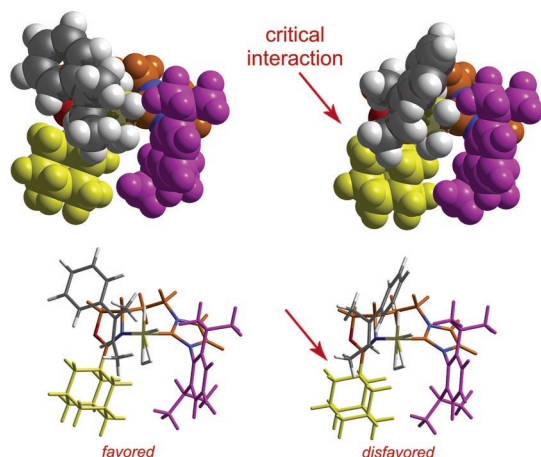


**Figure 1.** Space-filling and stick models for diastereomeric intermediates **1'**, where the alkene is (*E*)-2-phenylbut-2-ene-coordinated via the most favorable enantioface and the disfavored one.

were only accumulated for Ar = 4-MeOC<sub>6</sub>H<sub>4</sub> (when necessary to facilitate separation of the enantiomers via chiral GC),<sup>9,10</sup> but the computational data used Ar = Ph (to avoid complications caused by conformers of the OMe group). Even ignoring this difference, we consider the agreement between the virtual and experimental data to be exceptionally good.

Initially, reduction of COD and dissociation of the hydrogenated product produces several vacant sites. Alkenes can coordinate to any site other than those bound by the asymmetric ligand. To estimate the steric and electronic effects in the real catalyst, one 2-methylbut-2-ene was introduced to bond to these sites, while others are saturated with one H<sub>2</sub> and two hydrides. Extensive conformational searching indicated that when the alkene was coordinated trans to the carbene, as in **1c** and **1'**, it gave a structure that was  $\geq 10.5$  kcal mol<sup>-1</sup> more stable than other coordination sites.

Using the nomenclature shown in Scheme 2, the alkene-R<sup>2</sup> substituent encounters most steric interactions with the adamantyl of the oxazoline ligand. Those steric interactions decrease in the order R<sup>2</sup>  $\gg$  R<sup>1</sup> > Ph  $\gg$  R<sup>3</sup>. Figure 1 shows space-filling models for intermediates **1'** with (*E*)-2-phenylbut-2-ene (Table 1, entry 1), with the Ir coordinated to both enantiofaces. The  $\Delta\Delta G^\ddagger$  value between paths for the two enantiomers primarily stems from interactions at the monosubstituted end of that alkene, but imbalanced steric influences on Ph/Ar and R<sup>1</sup> substituents also have an effect. These considerations explain why the  $\Delta\Delta G^\ddagger$  value is less for 2-phenylbut-1-ene (entry 3) than for (*E*)-2-phenylbut-2-ene (entry 1); because the former alkene does not have a substituent at the most hindered position, the less powerful secondary effects

dominate. This also explains why the  $\Delta\Delta G^\ddagger$  for (*E*)-2-phenylbut-2-ene is 1.48 kcal mol<sup>-1</sup> larger than that for (*Z*)-2-phenylbut-2-ene (entries 1 and 2); in the former case, the substituents occupy the least-crowded positions, whereas in the latter, the methyl group at the R<sup>2</sup> position forces a suboptimal R<sup>1</sup>/Ph arrangement.

The  $\Delta\Delta G_{\text{int}}^\ddagger$  values in Table 1 reflect the same trends as the  $\Delta\Delta G^\ddagger$  data. This is significant since locating transition states (hence calculating  $\Delta\Delta G^\ddagger$ ) is a challenge. Furthermore, using  $\Delta\Delta G_{\text{int}}^\ddagger$  avoids the questions of which TS (TS-1' or TS-2') is rate determining as they have similar energies in the system with the full ligand. As a further test of the validity of this approach, it was applied to (*E*)-1,2-diphenylpropene. A huge predicted  $\Delta\Delta G_{\text{int}}^\ddagger$  of 8.16 kcal mol<sup>-1</sup> was obtained, and this matches the near-perfect enantioselectivity observed.<sup>9,10</sup>

These calculations provide a working model for enantioselective hydrogenations via catalyst **A**. It is a delicately balanced system in which the alkene is driven trans to the carbene, where it interacts primarily with the oxazoline adamantyl substituent. Conversely, hydrogen is directed past the 2,6-diisopropylphenyl carbene substituent by the trans effect of the oxazoline ligand. These electronic factors dominate, but they are reinforced by steric effects that ultimately define the enantioface selectivities given these directions of approach. Initial calculations for a typical phosphine oxazoline system by others<sup>12</sup> and by us (Supporting Information) indicate similar electronic effects prevail, but cleavage of dihydrogen via  $\sigma$ -metathesis may not be as important.

**Acknowledgment.** Financial support for this work was provided by the Robert Welch Foundation (A-648) and the National Science Foundation (CHE 98-00184 and MRI 02-16275).

**Supporting Information Available:** Computational methods, the mechanistic pathways examined, and the energies calculated. This material is available free of charge via the Internet at <http://pubs.acs.org>.

## References

- Crabtree, R. *Acc. Chem. Res.* **1979**, *12*, 331–337.
- Lightfoot, A.; Schneider, P.; Pfaltz, A. *Angew. Chem., Int. Ed.* **1998**, *37*, 2897–2899.
- Pfaltz, A.; Blankenstein, J.; Hilgraf, R.; Hormann, E.; McIntyre, S.; Menges, F.; Schonleber, M.; Smidt, S. P.; Wustenberg, B.; Zimmermann, N. *Adv. Synth. Catal.* **2003**, *345*, 33–43.
- Drury, W. J., III; Zimmermann, N.; Keenan, M.; Hayashi, M.; Kaiser, S.; Goddard, R.; Pfaltz, A. *Angew. Chem., Int. Ed.* **2004**, *43*, 70–74.
- Cozzi, P. G.; Menges, F.; Kaiser, S. *Synlett* **2003**, 833–836.
- Xu, G.; Gilbertson, S. *Tetrahedron Lett.* **2003**, *44*, 953–955.
- Tang, W.; Wang, W.; Zhang, X. *Angew. Chem., Int. Ed.* **2003**, *42*, 943–946.
- Gaussian 03 was used to fully optimize all structures, and then frequencies were analytically computed at the same level to confirm they were minima or transition states, as appropriate. Thermodynamic functions were calculated at 298.15 K and 1 atm. In the B3LYP calculations, a modified LANL2DZ with one *f*-function was used for the iridium atom. Frisch, M. J.; Trucks, G. W.; Schlegel, H. B.; Scuseria, G. E.; Robb, M. A.; Cheeseman, J. R.; Montgomery, J. A., Jr.; Vreven, T.; Kudin, K. N.; Burant, J. C.; Millam, J. M.; Iyengar, S. S.; Tomasi, J.; Barone, V.; Mennucci, B.; Cossi, M.; Scalmani, G.; Rega, N.; Petersson, G. A.; Nakatsuji, H.; Hada, M.; Ehara, M.; Toyota, K.; Fukuda, R.; Hasegawa, J.; Ishida, M.; Nakajima, T.; Honda, Y.; Kitao, O.; Nakai, H.; Klene, M.; Li, X.; Knox, J. E.; Hratchian, H. P.; Cross, J. B.; Bakken, V.; Adamo, C.; Jaramillo, J.; Gomperts, R.; Stratmann, R. E.; Yazyev, O.; Austin, A. J.; Cammi, R.; Pomelli, C.; Ochterski, J. W.; Ayala, P. Y.; Morokuma, K.; Voth, G. A.; Salvador, P.; Dannenberg, J. J.; Zakrzewski, V. G.; Dapprich, S.; Daniels, A. D.; Strain, M. C.; Farkas, O.; Malick, D. K.; Rabuck, A. D.; Raghavachari, K.; Foresman, J. B.; Ortiz, J. V.; Cui, Q.; Baboul, A. G.; Clifford, S.; Cioslowski, J.; Stefanov, B. B.; Liu, G.; Liashenko, A.; Piskorz, P.; Komaromi, I.; Martin, R. L.; Fox, D. J.; Keith, T.; Al-Laham, M. A.; Peng, C. Y.; Nanayakkara, A.; Challacombe, M.; Gill, P. M. W.; Johnson, B.; Chen, W.; Wong, M. W.; Gonzalez, C.; Pople, J. A. *Gaussian 03*, revision B.04; Gaussian, Inc.: Wallingford, CT, 2004.
- Powell, M. T.; Hou, D.-R.; Perry, M. C.; Cui, X.; Burgess, K. *J. Am. Chem. Soc.* **2001**, *123*, 8878–8879.
- Perry, M. C.; Cui, X.; Powell, M. T.; Hou, D.-R.; Reibenspies, J. H.; Burgess, K. *J. Am. Chem. Soc.* **2003**, *125*, 113–123.
- Herrmann, W. A. *Angew. Chem., Int. Ed.* **2002**, *41*, 1290–1309.
- Brandt, P.; Hedberg, C.; Andersson, P. *Chem.—Eur. J.* **2003**, *9*, 339–347.

JA044240G